Title

Inhibiting Translation Elongation with SVC112 Suppresses Cancer Stem Cells and Inhibits Growth in Head and Neck Squamous Carcinoma

Journal

Cancer Research, 80(5)

ISSN

0008-5472

Authors

Keysar, Stephen B
Gomes, Nathan
Miller, Bettina
et al.

Publication Date

2020-03-01

DOI

10.1158/0008-5472.can-19-3232

Peer reviewed

Published in final edited form as:

Cancer Res. 2020 March 01; 80(5): 1183–1198. doi:10.1158/0008-5472.CAN-19-3232.

Inhibiting translation elongation with SVC112 suppresses cancer stem cells and inhibits growth in head and neck squamous carcinoma

Stephen B. Keysar[1], **Nathan Gomes**[2], **Bettina Miller**[1], **Brian C. Jackson**[1], **Phuong N. Le**[1], **J. Jason Morton**[1], **Julie Reisinger**[1], **Tugs-Saikhan Chimed**[1], **Karina E. Gomez**[1], **Cera Nieto**[1], **Barbara Frederick**[2], **Gijsbertus J. Pronk**[2], **Hilary L. Somerset**[3], **Aik-Choon Tan**[1,4], **Xiao-Jing Wang**[3,5], **David Raben**[6], **Tin Tin Su**[2,7], **Antonio Jimeno**[1,5]

[1]Division of Medical Oncology, Department of Medicine, University of Colorado School of Medicine (UCSOM), CO, 80045

[2]SuviCa, Inc., Boulder, CO

[3]Department of Pathology, UCSOM and VA Medical Center, CO

[4]Department of Biostatistics and Informatics, University of Colorado School of Public Health, CO, 80045

[5]Gates Center for Regenerative Medicine, UCSOM

[6]Department of Radiation Oncology, UCSOM

[7]Department of Molecular, Cellular, and Developmental Biology, University of Colorado Boulder, CO, 80309

Abstract

Cancer stem cells (CSCs) drive growth, therapy resistance, and recurrence in head and neck squamous cell carcinoma (HNSCC). Regulation of protein translation is crucial for normal stem cells and CSCs; its inhibition could disrupt stemness properties, but translation inhibitors are limited clinically due to toxicity. SVC112 is a synthetic derivative of bouvardin, a plant-derived translation elongation inhibitor. SVC112 had greater anti-proliferative effects on HNSCC cells compared to the FDA-approved translation inhibitor omacetaxine mepesuccinate (HHT). SVC112 preferentially inhibited cancer cells compared to patient-matched cancer associated fibroblasts, while HHT was equally toxic to both. SVC112 reduced sphere formation by cell lines and CSCs. SVC112 alone inhibited the growth of patient-derived xenografts (PDXs), and SVC112 combined with radiation resulted in tumor regression in HPV-positive and HPV-negative HNSCC PDXs.

Corresponding Author: Antonio Jimeno M.D., Ph.D., Professor of Medicine/Oncology, and Otolaryngology, University of Colorado Cancer Center, and Gates Center for Regenerative Medicine, University of Colorado School of Medicine, 12801 East 17th Avenue, Room L18-8101B, Aurora, CO 80045, USA. Phone: 303-724-2478. Antonio.Jimeno@ucdenver.edu.; Tin Tin Su Ph.D., Professor of Molecular, Cellular & Developmental Biology, University of Colorado Boulder, 347 UCB, Gold Biosciences Building, Boulder, CO 80309, USA. Phone: 303-735-3245. Tin.Su@colorado.edu.

Disclosure of Potential Conflicts of Interest: N.G. and B.F. are employees of SuviCa, Inc. T.T.S., G.J.P., D.R., and A.J. declare patent/stock/stock options ownership in SuviCa, Inc.

Data and materials availability: Materials will be shared per the University of Colorado's Office for Technology Transfer policies and Institutional Review Board.

Notably, CSC depletion after SVC112 correlated with tumor response. SVC112 preferentially impeded ribosomal processing of mRNAs critical for stress response, and decreased CSC-related proteins including Myc and Sox2. SVC112 increased cell cycle progression delay and slowed DNA repair following radiation, enhancing colony and sphere formation radiation effects. In summary, these data demonstrate that SVC112 suppresses CSC-related proteins, enhances the effects of radiation, and blocks growth of HNSCC PDXs by inhibiting CSCs.

Keywords

Head and neck squamous cell carcinoma; SVC112; cancer stem cells; patient-derived xenografts; protein synthesis

INTRODUCTION

Head and neck squamous cell carcinoma (HNSCC) incidence has increased due to the rise in HPV-related tumors (1,2), and radiation therapy remains a mainstay of both front line and post-surgical management. Given current treatment failures and toxicity, more effective therapies are needed. Cancer stem cells (CSCs) sit atop the hierarchical tumor model and are the candidate population that sustains tumor growth, are resistant to therapy, and drive repopulation after treatment (3). We recently defined CSCs across HNSCC subtypes (4), and a concerted effort is underway to identify and target conserved cellular processes and signaling pathways that maintain CSCs (5,6). Tissue stem cells (SCs) are maintained through tight regulation of protein synthesis (7), and there is growing evidence that translation regulates the CSC phenotype (8). Like normal stem cells, the CSC phenotype require a discrete set of factors (e.g. Myc, Sox2) (9) that are challenging to target (10).

The Myc protein has a short half-life (20-30min) (11), suggesting Myc can be targeted, and depleted quickly, through the inhibition of *de novo* protein synthesis (12). We recently showed that the Sox2 pluripotency factor is regulated at the point of translation (4), and also has a relatively short half-life (~5h) (13,14), which supports that blocking translation may target CSCs (15). The dual reliance on protein synthesis to maintain core CSC factors and specific effectors of CSC signaling led us to exploit this vulnerability, or protein addiction. The translational elongation inhibitor bouvardin, identified in a *Drosophila* regeneration screen (16), impacted primordial cell repopulation following radiation (17) by locking eukaryotic elongation factor 2 (eEF2) to ribosomes (18). Improvement of bouvardin yielded the fully synthetic derivative SVC112 (SuviCa Inc., Boulder, CO). Unlike translation initiation inhibitors (12,15), elongation inhibitors such as SVC112 block both cap-dependent and cap-independent internal ribosome entry site (IRES)-dependent translation. Cap-independent translation is preferentially activated during stress and hypoxia for mRNAs containing an IRES, which include those encoding Myc and Cyclin D1 (19–21). Translation elongation inhibition was validated by omacetaxine mepesuccinate (semisynthetic homoharringtonine [HHT]), which is FDA-approved in chronic myeloid leukemia (CML) where it suppresses the BCR-ABL fusion protein, however its use is limited by toxicity (22).

Here we explored how protein elongation inhibition with SVC112 impacts basic cell features such as viability and proliferation and also more complex properties such as sphere

formation, response to radiation damage, and *in vivo* tumor growth, using established HNSCC cell lines, patient-matched HNSCC cell lines and cancer associated fibroblasts (CAFs), and patient-derived xenografts (PDX). SVC112 had an improved therapeutic index and preferentially targeted cancer cells compared to patient-matched CAFs, as opposed to HHT that inhibited growth of cancer and non-cancer cells alike. SVC112 enhanced radiation effects in HNSCC cells but not in non-transformed cells, suppressed Myc, Cyclin D1, and Sox2 proteins, and inhibited sphere formation. SVC112 alone and combined with radiation inhibited HPV-negative and HPV-positive PDX tumors. This is the first report of a translation elongation inhibitor that reduces HNSCC PDX growth by reducing the *in vivo* CSC fraction beyond a critical threshold.

METHODS

Study approval

Studies involving human subjects were approved by the Colorado Multiple Institutional Review Board (COMIRB-08-0552). Informed written consent was obtained from all patients whose tissues were used for this study. The University of Colorado Institutional Animal Care and Use Committee approved all mouse experiments.

Cell lines

013C, 036C, 049C, and 067C cells were derived and maintained as previously described (4). 013CAF, 036CAF, and 067CAF cells were derived from tumor tissue using DMEM with 10% FBS, penicillin (200units/mL), and streptomycin (200ug/mL) and immortalized using SV40 LgT and hTERT expression (23). To generate resistant cell lines, 013C and 036C were cultured in media containing increasing concentrations of drug until they grew normally at 1,000nM and 100nM respectively. Established HNSCC cell lines (e.g. Fadu, Detroit562) were obtained by SuviCa from Drs. David Raben and Barbara Frederick, University of Colorado. Cell lines were authenticated by DNA fingerprinting (STR analysis) before and during use.

Compounds and irradiation

Homoharringtonine (HHT) was acquired commercially (Sigma, St. Louis, MO). Cells were irradiated in a Fa xitron Cabinet X-ray System Model RX-650 (Lincolnshire, IL) at 115 kv and 319 cGy/min.

SVC112 pharmacological analysis

Meta Br-N-29-H derivative of RA-VII (PubChem CID: 3034401) was synthesized, characterized by 1D and 2D NMR and by LC-MS, and used at 98% or greater purity (by HPLC).

Pharmacokinetics studies

These were performed by WuXi Apptec (Shanghai, China) under contract to SuviCa, Inc. Female CD-1 mice were dosed with 40mg/kg SVC112. Vein blood was drawn and plasma levels quantified by LC-MS/MS.

Gene (cDNA) overexpression

For gene overexpression experiments HEK293T cells were transfected with an empty (control) pMICH-mCherry retroviral vector, or vector containing cDNA for SOX2, and the pCL-Ampho packaging plasmid. 013C, 036C, 049C, and 067C cells were transduced with the resulting viral media and cells were selected by mCherry expression (FACS).

Toxicology and histopathology analysis

The toxic effect of SVC112 was assessed in non-tumor bearing female Balb/C mice. The studies were performed under a contract at the University of Colorado Pharmacology Shared Resource, University of Colorado Cancer Center. Mice were randomly assigned to treatment groups and treated with vehicle or SVC112 (IP at 60mg/kg, q6h x 2, once per week). Vehicle solution (1.03% D-α-Tocopherol polyethylene glycol 1000 succinate (TPGS) and 1% poloxamer in water) was dosed at 100μL per 25g body weight at the time of SVC112 dosing. SVC112 nanosuspension dosing solution was freshly prepared and dosed IP at 60mg/kg (q6h x 2, once per week) at 100μL per 25g body weight. Body weight was measured thrice weekly to grossly assess toxicity. Organs were collected 24h from the last SVC112 dose.

Animal anesthesia and pain management

For cell injection and PDX tumor implantation animals were anesthetized with Isoflurane (induction at 5%, maintained at 1-2%). In preparation for surgical implantation of PDX tumor tissue, and for 48h following the procedure, animals received buprenorphine injections (1mg/kg) every 12h.

PDX efficacy studies

PDX generation and characterization was previously reported (24). Tumor pieces were implanted on both flanks of 6 to 10-week-old female Athymic Nude-*Foxn1*^{nu} mice (Envigo, Denver, CO). Cases (4th-8th generation) were expanded into larger cohorts. For efficacy studies, anesthetized mice were shielded leaving only the flank tumors exposed, and irradiated (RS-2000 irradiator, Rad Source Technologies, Buford, GA) at 115cGy/min, twice weekly (3Gy) for four weeks. SVC112 was delivered IP (60mg/kg) immediately following radiation treatment and again 6h later. Tumors were measured twice weekly.

Nonadherent sphere formation

Cell lines or PDX-derived CSCs were plated in ultra-low attachment 96 well plates at a concentration of 3x10^3 (cell lines) or 1x10^4 (PDX CSCs) per well in serum-free DMEM/F12 media supplemented with 10ng/ml EGF and 10ng/ml bFGF. Media was supplemented 4, 7 and 10 days following cell seeding. Cells were allowed to form spheres for 10 or 14 days for cell lines or CSCs respectively. All spheres (>50μm) in a well were manually imaged, counted and measured (diameter) using a Zeiss Axio Observer Z1 inverted microscope (Zeiss software Rel. 4.8).

Cell cycle analysis

For bromodeoxyuridine (BrdU) labeling, cells were incubated for 1h in media containing 10μM BrdU, then washed twice with warm PBS, and fresh media was added. Cells were immediately irradiated followed by the addition of SVC112. Cells were collected at multiple time points following irradiation, suspended in 2ml of cold PBS, and fixed by the dropwise addition of cold 100% ethanol to 7ml total volume. BrdU incorporation was labeled with anti-BrdU-Alexa488 antibodies (#B35189, Invitrogen, Carlsbad, CA) for 25min. For analysis, cells were suspended in 10μg/ml propidium iodide (PI) in PBS plus 5μl Rnase A per ml. For PI only cell cycle analysis, fixed cells were suspended in 50μg/ml PI in PBS plus 5μl Rnase A per ml. Resulting histograms were analyzed by Modfit LT software, v3.3 (BD, San Jose, CA).

Protein synthesis (Click-iT) assays

To quantify de novo protein synthesis in HNSCC cell lines, cells were incubated in methionine-free media (Invitrogen) for 1 h, followed by addition of L-azidohomoalanine (AHA, 50 μM final) (Invitrogen) and the indicated SVC112 drug concentrations for 2 hr, prior to harvest. Labeling of de novo proteins containing AHA with Tetramethylrhodamine was performed using Click-iT Protein Analysis Detection Kit (Invitrogen) following manufacture's protocols and as previously described (18).

For early-passage HNSCC cell lines the methionine analog incorporation assay was completed following the manufacturer's instructions (Invitrogen) unless noted below. Cells were seeded in 96-well plates in normal growth media and incubated for 48h. Cells were then washed with PBS before adding L-methionine free DMEM (#21013024, Thermo, Waltham, MA supplemented with 53ng/L L-cystine and 584 ng/L L-glutamine) containing methionine analog (L-Homoproparglyglycine [HPG]) and either control vehicle, SVC112 or homoharringtonine (HHT). Cells were then incubated for 1.5h before fixation and labeling for HPG incorporation. HPG incorporation was assessed by measuring fluorescence intensity (Alexa-488) for 30 cells (10 cells for 3 replicate regions within each well) per treatment condition, normalized to background using a Zeiss Axio Observer Z1 inverted microscope (Zeiss software Rel. 4.8).

Western blotting

Cell pellets were lysed in 30-100μl RIPA lysis buffer containing 5μl/ml PMSF. Protein concentration was measured using Bradford Assay and the ELx800 absorbance microplate reader (BioTek) according to the manufacturer's instructions. 30ng of protein was loaded per well into NuPage Novex 4-12% Bis-Tris Midi Gel (Life Technologies, Carlsbad, CA), transferred using the iBlot Gel Transfer Stack System (Life Technologies). Primary Antibodies: Myc (#5605S, Cell Signaling, Danvers, MA), Cyclin D1 (#2978S, Cell Signaling), Sox2 (#3579S, Cell Signaling), eEF2 (#2332S, Cell Signaling), Actin (4968S, Cell Signaling), and Vinculin (#ab129002, Abcam). Secondary anti-rabbit IgG was purchased from Jackson ImmunoResearch (West Grove, PA), and used at a 1:50,000 dilution. Signal was visualized using Immobilon Western chemiluminescent HRP substrate (EMD Millipore) on x-ray film. Quantification of relative protein levels was completed using ImageJ software version 1.5 (National Institutes of Health, imagej.nih.gov).

Immunofluorescence analysis of γH2AX foci

Cells were seeded in chamber slides and incubated for 2 days before irradiation. Slides were fixed in 4% paraformaldehyde at 0, 0.5, 2, and 6h following 4Gy x-ray treatment. Slides were washed with PBS+0.5% Tween20, permeabilized in 0.2% Triton X-100 for 10min at room temperature, and blocked in PBS+5% milk for 1h. Samples were labeled in PBS +1%BSA with the primary antibody mouse anti-γH2AX (#05-636, Millipore, Burlington, MA) at 1:500 for 1.5h, and secondary goat anti-mouse-Alexa488 (#A11029, Thermo) for 1.5h. ProLong Gold antifade with DAPI (#P36931, Invitrogen) was added to slides before covering. Nuclei were randomly imaged by DAPI staining using a Zeiss Axio Observer Z1 inverted microscope (Zeiss software Rel. 4.8) at 1,008x magnification. Foci (punctate fluorescent nuclear staining) were scored as foci/nuclei and 50 nuclei were assessed per treatment. Results presented are from three independent experiments.

Immunohistochemistry (IHC)

Primary antibodies and dilutions; 1:200 Cleaved caspase-3 (#9664, Cell Signaling), 1:100 Ki67 (#RM-9106-S1, Thermo), 1:200 Myc (#AB32072, Abcam), and 1:100 Cyclin D1 (#2978, Cell Signaling). Slides were de-paraffinized and re-hydrated in graded concentrations of alcohol by standard techniques before antigen retrieval in citrate buffer pH 6.0 (#S1699, Dako/Agilent) for Myc, Cyclin D1, and Cleaved Caspase-3 at 121^{o}F for 10 min. All staining was done in a Dako Autostainer, and slides were incubated in Dual Endogenous Enzyme Block (#S2003, Dako/Agilent) for 10min, and in protein free blocking solution (#X0909, Dako/Agilent) for 20 minutes, and followed by the appropriate dilution of primary antibody (60min at room temperature). Staining was developed using the following conditions: EnVision + Dual Link System HRP (#K4061, Dako/Agilent) for 30min and substrate-chromogen (DAB+) Solution (#K3468, Dako/Agilent) for 5 min. Slides were then counterstained with Automated Hematoxylin (#S3301, Dako/Agilent) for 10 min.

To assess changes in tumor tissue following treatment, four independent tumors per treatment arm were HE stained and then ten random regions of the proliferating tumor edge were imaged (5X) using a Zeiss Axio Observer Z1 inverted microscope. Proliferating cell depth for each image was measured using Zeiss software Rel. 4.8..

To quantify changes Myc following treatment, four tumors per treatment arm were analyzed by Myc IHC staining. Three random images of viable tumor were scored manually (number of Myc positively stained nuclei per 100 nuclei).

For spheres treated with SVC112, ImageJ Fiji software was used to measure changes in Myc and Cyclin D1 IHC staining (DAB intensity). Individual spheres were gated as regions of Interest. Image color was deconvoluted and the color 2 (DAB spectrum) channel was analyzed for mean intensity of the image (0=full brown, 255=white). DAB optical density (OD) was calculated by OD = log(max intensity/mean intensity). For each treatment, DAB intensity for ten spheres, five from two independent replicates, was quantified.

Ribosome profiling (Ribo-seq)

Cells (013C, 049C, 067C) were seeded in 10cm cell culture dishes and incubated for 48h to reach ~75% confluency. Cells were then treated with media containing DMSO (control) or SVC112 (1,000nM) for 6h before harvesting. Cells were collected and libraries were generated following the manufacturer's (Illumina) instructions in the Mammalian TruSeq Ribo Profile Reference Guide. Isolated total mRNA fragments and ribosomal protected mRNA fragments (RPF) were sequenced on an Illumina HiSEQ instrument at the University of Colorado Cancer Center's Genomic Core. Data processing and analysis were completed as previously reported (25).

Statistical analyses

Experiments were compared by two-tailed Student's *t* test. Kaplan-Meier survival curves were analyzed by log-rank Mantel-Cox test. Correlation between CSC changes and tumor response was analyzed by linear regression. Calculations were done using GraphPad Prism version 8.0. Data are represented graphically as mean ±SD or ±SEM. GSEA estimates statistical significance by a modified Kolmogorov-Smirnov permutation test. *P* of less than .05 were statistically significant. All statistical tests were two-sided.

RESULTS

SVC112 inhibits protein synthesis, proliferation, and enhances radiation effects

SVC112, a fully synthetic derivative of the cyclic hexapeptide bouvardin (Fig. 1A). SVC112 inhibits *in vitro* cap-independent translation of capless luciferase mRNA using rabbit reticulocyte lysates (IC50=81±16nM) (Fig. 1B). SVC112 blocked the release of eEF2 from the ribosome (Fig. 1C) like bouvardin (18), as measured by immunoprecipitation of eEF2 with ribosomal protein l13a (Rpl13a). SVC112 inhibited *de novo* protein synthesis in HNSCC cells (Fig. 1D), which led to the rapid depletion of Cyclin D1 (26) and Myc proteins (Fig. 1E; Supplementary Fig. S1A). SVC112 inhibited growth in 19 HNSCC lines with an average IC50 of 155nM (Fig. 1F) and SVC112 enhanced the anti-clonogenic effect of radiation (Fig. 1G **and** H; Supplementary Fig. S1B; Supplementary Table S1). The dose-modifying factor (DMF) is a measure of how the anti-biological effects (e.g. clonogenicity) of a radiation dose are enhanced by drug (e.g. SVC112) treatment (27). For multiple SVC112 doses the DMF was >1 in cancer cells, but near or below 1 in four non-transformed normal lines (Fig. 1I), suggesting that SVC112 enhances radiation only in cancer cells.

SVC112 has a selective anti-proliferative effect on low passage HNSCC cells

We assessed SVC112 antiproliferative effects in four low passage cell lines, three of which have patient-matched CAFs (013CAF, 036CAF, 067CAF) as a non-transformed comparison. 036C, 067C, 049C, and 013C had IC50s of 3.8nM, 9.3nM, 24.1nM, and 50.5nM, respectively (Fig. 1J **and** K; Supplementary Fig. S1C), and 036C, 067C, and 049C were 13.9-, 2.1-, and 1.7-fold more sensitive to SVC112 than HHT. Patient-matched 036CAFs and 067CAFs were 3.8- and 5.6-fold less sensitive to SVC112 than cancer cells, while there was a lesser or opposite effect for HHT (Fig. 1J **and** K). Sensitivity did not correlate with cell proliferation (Supplementary Fig. S1D), and SVC112 induced a dose-dependent

reduction in new protein synthesis in 036C, 067C, and 013C (Fig. 1L). While SVC112 and HHT both have substantial anti-proliferative effects at nanomolar concentrations, SVC112 has a superior therapeutic index (relatively sparing normal cells) at doses achievable *in vivo* (Supplementary Fig. S1E). This has significant implications from both a selectivity of action and a translational perspective.

SVC112 inhibits tumor sphere growth

We next assessed SVC112 effect on tumor spheres, which is a standard *in vitro* method to assess CSC properties. SVC112 suppressed Myc and Cyclin D1 in pre-formed spheres (Fig. 2A). Seeding cells in media containing SVC112 (1,000nM) blocked sphere formation ($P<.001$) by 100%, 79%, 74%, and 48% in 036C, 067C, 013C, and 049C, respectively. While 100nM and 1,000nM SVC112 also decreased the size of resulting 067C spheres, 013C sphere size increased at 100nm and was unaffected at 1,000nM ($P=.320$) (Fig. 2B). SVC112 and HHT had a similar impact at 100nM, while 1,000nM HHT blocked nearly all sphere formation. SVC112 (100nM) increased sphere inhibition by radiation in 036C, and 067C cells, with a lower effect in 049C, and no impact in 013C (Supplementary Fig. S1F **and** G).

We sorted stringently defined CSCs (Aldefluor^{+}CD44^{high}) from PDX tumors for *ex vivo* non-adherent cultures. CSCs had higher Myc and Sox2 levels compared to non-CSC tumor cells, and addition of SVC112 to non-adherent CSC cultures suppressed Myc and Sox2 proteins (Supplementary Fig. S1H **and** I). SVC112 (1,000nM) blocked sphere formation by CUHN036 ($P=.001$) and CUHN004 ($P=.001$) CSCs, while CUHN013 ($P=.001$) CSCs formed fewer, albeit normal-sized spheres (Fig. 2C).

SVC112 alone and with radiation inhibits *in vivo* tumor growth

We conducted PDX efficacy studies to explore the SVC112 inhibitory potential on CSCs, both alone and with radiation, in a preclinical setting that is stringent and as close as possible to a patient. CUHN013 and CUHN036 PDXs were chosen based on the divergent effects of SVC112 on matched (013C, 036C) cells *in vitro*. CUHN004 and CUHN047 were derived from a relapsed HPV-negative subject and a HPV-positive patient, respectively (Supplementary Table S2). Treatment groups were control, twice weekly radiation (3Gy), twice weekly SVC112, or the combination of radiation followed by SVC112. Radiation alone suppressed growth in CUHN036 (T/C=0.31±0.10, $P<.001$) and CUHN047 (T/C=0.27±0.09, $P<.001$). SVC112 alone suppressed growth in CUHN036 (T/C=0.45±0.12, $P=.005$) and CUHN047 (T/C=0.37±0.07, $P<.001$), and radiation plus SVC112 inhibited growth in CUHN047 (T/C=−0.02±0.03, $P<.001$), CUHN036 (T/C=0.08±0.08, $P<.001$), and CUHN004 (T/C=0.19±0.05, $P<.001$) (Fig. 3A). Combination treatment resulted in complete regression in six out of ten CUHN047 tumors and four of twelve CUHN036 tumors by day 28. After ending treatment, six of eight CUHN036 tumors continued to regress and did not regrow (Fig. 3B **and** C; Supplementary Fig. S2A). CUHN013 did not respond to any treatment (Fig. 3A). Initial studies treating CUHN013 and CUHN036 once weekly generated less dramatic inhibition in CUHN036 ($P=.003$), which suggests dose dependency (Supplementary Fig. S2B). Weekly SVC112 increased inhibition of FaDu xenografts when combined with radiation (2Gy twice weekly) and cisplatin (1mg/kg weekly) (Supplementary

Fig. S2C). Significant weight loss compared to control animals was only observed in the combination arm of animals bearing CUHN013 tumors treated twice weekly (*P*=.003) (Supplementary Fig. S2D), and no abnormal histopathology was observed in mice treated with SVC112 for 4 weeks (Supplementary Table S3).

Histological analysis of tumors from end of treatment (day 28) noted increased keratinization and necrosis as well as fewer viable tumor cells in all treatment arms. Notably, combination treated CUHN036 (*P*<.001) and CUHN047 (*P*<.001) tumors had only thin rims of viable tumor remaining (Fig. 3D–F). SVC112 suppressed Myc (IHC) in CUHN036 (*P*<.001), and combination treatment suppressed Myc in CUHN036 (*P*<.001) and CUHN047 (*P*<.001) tumors (Fig. 3G **and** H). Cleaved caspase-3 increased in irradiated or combination treated tumors (CUHN036, CUHN047, CUHN004, but not SVC112 treated tumors, suggesting the SVC112 mechanism of action is not apoptosis (Supplementary Fig. S2E). These results showed *in vitro* and *in vivo* consistency for patient-matched CUHN013 and CUHN036 PDX tumors compared to 013C and 036C cells respectively.

SVC112 decreases CSC number *in vivo*

To assess a potentially anti-CSC effect *in vivo*, we analyzed the CSC subpopulation (ALDH $^{+}$CD44^{hi}) within tumors following treatment, noting that CUHN013 had the highest baseline CSC population. Radiation decreased the CSC fraction only within CUHN036 tumors \, while SVC112 decreased CSCs in all four cases. Combination treatment decreased CSCs by 10.4-, 7.6-, and 7.9-fold in CUHN036 (*P*<.001), CUHN047 (*P*=.012), and CUHN004 (*P*=.018) respectively, but only 2.4-fold in CUHN013 (*P*=.005). Tumor inhibition was associated with lowering the CSC population below 1% (Fig. 4A **and** B). There was a strong relationship (measured by linear regression) between the fold change reduction of CSCs *in vivo* (CSC-FC) and tumor response following SVC112 treatment (alone and with radiation) both by pooled treatment arms (R^2=0.543, *P*=.037) (Fig. 4C) or by individual tumors (R^2=0.224, *P*=.002) (Fig. 4D), which suggests that surpassing a threshold in reducing CSCs is required to achieve tumor arrest.

SVC112 depletes proteins by influencing translation but not transcription

In order to understand the biological effects of SVC112 on tumors, and specifically how it impedes normal ribosomal processing of transcripts, we sequenced ribosome protected mRNA fragments (RPF) in control and SVC112-treated cells (013C, 049C, 067C; 6h exposure) using Ribo-seq. Seventy RPFs were enriched >2-fold after normalization to RNA-seq across SVC112-treated cells, indicating they are captive in the ribosome; ten were related to cellular stress response (e.g. *DUSP1*, *MAFF*, *DUSP5*, *ATF3*), four with TNFα signaling (e.g. *TNFAIP2*, *TRAF1*), four with NF-κB signaling (e.g. *NFKBIA*, *RELB*, *NFKB2*), and four were ribosomal/translational proteins (*RPL18*, *RPS9*, *RPS16*, *EEF1D*) (Supplementary Fig. S3A). Ribo-seq identified 1699-, 666-, 346-, and 238-fold increases following SVC112 in captured RFPs of *SERTAD1, NUAK2, MAFF, and DUSP1* respectively, three of which (*SERTAD1*, *NUAK2, DUSP*1) have putative internal ribosome entry sites (IRES) within their transcribed mRNA sequence (Supplementary Fig. S3A). GSEA analysis of RPFs (captive mRNAs) identified hallmark pathways related to stress response, including *TNFα Signaling via NF-κB* and *p53 pathway* (Supplementary Fig.S3B).

Overall this indicates that SVC112 impedes ribosomal processing of mRNAs that are particularly critical for cancer cells, including IRES-containing response to cell stress and inflammation genes.

Acute SVC112 (24h) did not decrease the mRNA levels of Myc, Cyclin D1, or Sox2 (Supplementary Fig. S3C), supporting that SVC112 effects are post-transcriptional. SVC112 (10nM) significantly suppressed *ALDH1A1* mRNA (036C P=.008, 067C P<,001, 049C P<.001, 013C P=.001), which is transcriptionally regulated by the Sox2 protein (4). Global RNA-seq identified decreased transcription of GSEA hallmark pathways (*Myc Targets, Wnt β-catenin Signaling, Angiogenesis*), likely due to depletion of proteins like Myc by SVC112. Conversely, increased expression of *Apoptosis*, *p53 Pathway*, and *Epithelial to Mesenchymal Transition* signaling (Supplementary Table S4) was also noted.

SVC112 inhibits translation more potently in HNSCC cells than autologous non-cancer cells

To further assess the cancer selectivity of SVC112, we used three patient-matched pairs of HNSCC and CAF cell lines, and compared SVC112 to HHT. CAFs had similar (013CAF) or higher (036CAF, 067CAF) protein synthesis than their patient-matched cancer lines (Supplementary Fig. S4A). Both SVC112 and HHT suppressed translation in all cells by >85% at 100nM, though only SVC112 decreased protein synthesis by >50% in 036C (P<.001) and 067C (P<.001) cells at 1nM. 013C was the least sensitive requiring a 10-fold higher dose (10nM) to achieve ~50% inhibition. 036C and 067C were more susceptible (lower IC50s) to SVC112 than their patient-matched CAFs (Fig. 2C; Supplementary Fig. S4B).

SVC112 suppresses proteins associated with proliferation and CSC properties in HNSCC

Myc and Cyclin D1 have short half-lives (<1h) and are expressed at different levels in HNSCC cells, while eEF2 is higher in cancer cells compared to CAFs (Supplementary Fig. S4C **and** D). SVC112 decreased Cyclin D1 protein within 1h, which remained suppressed at 3h and 6h for all cell lines. Cyclin D1 levels started to recover by 24h in 013C, 049C, and 067C cells, but remained suppressed in 036C. Myc decreased in all lines within 1h, although complete suppression of Myc was slower (~6h) in 013C and 067C cells. Myc remained suppressed (>80% reduction) at 24h for 036C, 049C, 067C, but returned to >60% of baseline in 013C (Fig. 5A). SVC112 had no effect on eEF2 levels in cancer cell lines (Supplementary Fig. S4E). Following incubation (24h) with cells, transferred media containing SVC112 inhibited protein synthesis, proliferation, and suppressed protein levels like fresh drug, indicating SVC112 stability (Supplementary Fig. S4F–H). However, this suggests cells can recover protein synthesis even in the continued presence of inhibitor.

Protein depletion by SVC112 is reversible while effects on CSC properties are longer lasting

To test treatment reversibility cells were either maintained in SVC112-containing media (100nM) for 6h and 24h, or treated for 6h followed by an 18h washout period (6h: 24h). Myc and Cyclin D1 decreased with continuous exposure (6h or 24h) but returned to baseline within 18h following washout (6h: 24h) (Supplementary Fig. S5A). To assess the duration of

SVC112 inhibitory effects, cells were treated and then seeded (clonogenic, spheres) following washout periods of 6h, 24h, and 48h. Sustained reduction of clonogenicity and sphere formation was observed for 24-48h after SVC112 removal (Supplementary Fig. S5B–D).

When comparing the effect of SVC112 and HHT on Myc and Cyclin D1, sensitive strains had an idiosyncratic response (Supplementary Fig. S5E **and** F); in the less sensitive 013C (highest baseline levels of Sox2 and Myc; Supplementary Fig. S4C) HHT consistently achieved higher protein inhibition.

Resistant cell lines were generated by continuous culture in increasing concentrations of SVC112 until 036C and 013C cells proliferated normally (compared to DMSO treated controls) in 100nM and 1,000nM SVC112, respectively. Originating 013C cells were intrinsically resistant to SVC112 compared 036C, and continuous treatment generated a highly SVC112 resistant 013C strain. Both generated resistant cell lines were dramatically less sensitive to both growth and protein synthesis inhibition by SVC112, with no difference between chronically treated or cells washed out of drug seven days before assessment (Fig. 5B **and** C). Sphere forming potential significantly increased in resistant 036C ($P<.001$) and 013C ($P<.001$) resistant strains, and 036C resistant spheres were larger (Fig. 5D **and** E). There was no change in to the ability of HHT or radiation to inhibit growth or protein synthesis in SVC112-resistant cell lines (Fig. 5F **and** G; Supplementary Fig. S6A). Both resistant lines had increased Cyclin D1 levels, whereas resistant 013C had higher Sox2 and resistant 036C had lower eEF2 compared to control (Supplementary Fig. S6B **and** C).

Exogenous expression of Sox2 rescues the anti-sphering effects of SVC112

Since Sox2 has been previously shown to enable and enhance CSC properties in HNSCC, we assessed its ability to counter SVC112 effects. Forced Sox2 expression blunted the anti-sphering effects of 100nM SVC112 in three of four cell lines (036C $P=.004$, 049C $P<.001$, 013C $P<.001$). Sox2 expression did not rescue SVC112 sphering inhibition in 067C cells, but decreased the impact on sphere size ($P<.001$) (Fig. 6A; Supplementary Fig. S7A). Sox2 expression did not consistently alter total protein synthesis or the ability of SVC112 to inhibit protein synthesis (Fig. 6B; Supplementary Fig. S7B). Myc and Cyclin D1 baseline levels did not change with expression, and SVC112 continued to suppress their levels (Fig. 6C). Sox2 expression did not affect cell cycle kinetics following radiation and SVC112 (Supplementary Fig. S7C). Together, this suggests that the effects of Sox2 on SVC112 treatment is limited to its role as a stemness factor.

SVC112 enhances the effects of radiation by delaying DNA repair

To characterize radiation enhancement, we analyzed the cell cycle for 013C, 036C, 049C and 067C up to 48h after 4Gy±100nM SVC112. SVC112 alone increased the fraction of cells in G1/G0 phase by 12h in 049C ($P<.001$) and 24h in 013C ($P=.022$), 036C ($P=.011$) and 067C ($P=.003$) cells. Radiation induced G2/M arrest by 12h in all cell lines, but cells began cycling within 24h. SVC112 after radiation led to a persistent G2/M block at 36h and >48h in 013C and 036C cells, respectively (Fig. 7A **and** B; Supplementary Fig. S7D **and** E).

Cells were pulse-labeled with BrdU prior to treatment (4Gy±100nM SVC112). SVC112 decreased dividing (G1 phase) BrdU-positive 036C and 013C cells by 15.6- and 2.1-fold, respectively (Fig. 7C, black arrows). 12h following radiation, nearly all BrdU labeled cells were arrested in G2/M, which was delayed by SVC112 treatment; note BrdU-positive cells remaining in S phase (Fig. 7D, blue arrows). SVC112 decreased the number of BrdU-positive cells that had cleared the G2/M arrest at 24h after radiation by 7.8-fold in 036C and 2.8-fold in 013C. (Fig. 7D, red arrows). This data indicates that part of the SVC112 effect is by interference with checkpoint activation and recovery, and that 036C is more sensitive to these effects than 013C.

To assess SVC112 impact on DNA double strand breaks following radiation we next measured γH2AX foci formation finding that SVC112 alone or with radiation did not increase DNA double strand breaks (γH2AX foci formation). However, SVC112 significantly delayed the loss of γH2AX foci (DNA repair) at 2h (036C and 013C, $P<.001$) and 6h (036C and 013C, $P<.001$) post-radiation in both 013C and 036C (Fig. 7E **and** F). This data indicates SVC112 interferes with checkpoint activation and recovery, does not increase DNA damage, but delays DNA repair, which delays cell cycle recovery.

DISCUSSION

Aberrant translation can increase CSC-related proteins and properties (8,28), in contrast, tightly regulated translation maintains the balance between normal tissue SCs and proliferative progenitors (7). There have been significant efforts to target CSCs (5,6) and to leverage translation inhibition as therapy (12,15). HHT suppresses the BCR-ABL fusion protein (29) and depletes leukemia SCs more effectively than fusion-targeted tyrosine kinase inhibitors (30). Therefore, we tested the ability of SVC112 to suppress HNSCC CSCs and thus HNSCC growth.

SVC112 reduced translation more potently than HHT, which is likely due to differences in how each compound interacts with the ribosome; HTT binds to the ribosome A-site (31,32) whereas SVC112 locks eEF2 on the ribosome (18). HHT had a similar impact on patient-matched cancer cells and non-tumorigenic CAFs, whereas SVC112 had a superior therapeutic index, particularly at clinically achievable concentrations (10-100nM). Sparing normal tissues while blocking tumor growth is an ultimate therapeutic goal (33,34).

A key question is if SVC112 induces selective inhibition of specific transcripts, or if it impacts transcripts more critical to HNSCC. By sequencing total mRNAs and RPFs from SVC112-treated cells, we identified changes in gene expression and actively translated ORFs respectively. RNA-seq analysis identified decreased expression of Myc targets in treated cells, which follows the suppression of Myc by SVC112. Ribo-seq analysis of RPFs after treatment evidenced that transcripts of proteins related to inflammatory response pathways like TNFα/NF-κB signaling, as well as apoptosis and p53 pathways were captive in the ribosome at a dramatically higher proportion compared to RNA-seq also after SVC112. Of the top four genes with this translation/transcription discordance, three (*SERTAD1*, *DUSP1*, *NUAK2*) contained a putative IRES, suggesting they are regulated at the point of translation more so than transcription. DUSP phosphatases are of particular

interest since they negatively regulate MAPKs (35), which are known to decrease rapamycin-induced autophagy (36) and gemcitabine effect (37). Other putative targets of SVC112 preferentially captured in ribosomes included MAFF and ATF3 that are known stress response transcription factors and promote radioresistance (38,39), and TNFα/NF-κB signaling components, activated following cellular stress (40,41). Finally, we observed increased ribosome-association of ribosomal proteins, that activate the p53 pathway in response to ribosomal stress (42). Overall, these findings suggest that underlying the effect of SVC112 is the suppression of proteins that are critical for cancer cells, that is, SVC112 takes advantage of the protein addiction of HNSCC. Similar to how HHT suppression of BCR-ABL (29) depletes leukemic SCs (30), targeting CSC-related proteins in solid tumors using translation initiation inhibitors has been proposed (12,15). However, stress and hypoxia promote cap-independent translation of IRES containing mRNAs (e.g. Myc, Cyclin D1), which is not blocked by cap-dependent initiation inhibitors like HHT. Elongation inhibition by SVC112 significantly suppressed Myc, Cyclin D1 and Sox2 in HNSCC cells and CSCs *in vitro, ex vivo,* and *in vivo*. Sox2 maintains CSCs (4) and rescued cells from SVC112 anti-sphering effect, although it did not alter Myc/Cyclin D1 levels.

Tissue SC depletion leads to organ failure (e.g. cirrhosis, aplastic disease) (43,44) and we hypothesized that sufficient CSC depletion would inhibit tumors. Combination treatment significantly decreased CSCs in all four cases (>7-fold in responding cases, ~2-fold in resistant tumors) and CSC suppression below 1% was associated with tumor response. This may explain how, in addition to enhancing radiation efficacy in two radiation-sensitive cases, SVC112 increased radiation effectiveness in the resistant CUHN004. Despite a modest decrease in 013C sphering, SVC112 had no impact *in vivo*, likely because the CSC threshold was not achieved in CUHN013. These findings reinforce the importance of deploying adequately complex preclinical systems that avoid the over-estimation of efficacy seen with cell lines (45).

The tested PDXs covered the HNSCC spectrum by etiology (HPV-positive/-negative), response to therapy (radiation sensitive/resistant), and clinical stage (primary/relapse). We have reported that PDX susceptibility to approved agents such as cetuximab suggests they are representative and possibly predictive of patient outcomes (24). Overall, *in vivo* testing mirrored the *in vitro* results, and the models reproduced the radiation therapy susceptibility documented in the patients.

SVC112 inhibited translation elongation and preferentially blocked proliferation of HNSCC compared to non-cancer cells. SVC112 suppressed CSC-related proteins, resulting in decreased proliferation and sphere formation. In PDXs representative of the clinical spectrum of HNSCC, SVC112 inhibited growth and led to tumor regression when combined with radiation. The degree of CSC depletion in tumors was associated with response to SVC112 across PDXs tested. Exogenous Sox2 partially rescued the anti-sphering effects of SVC112, confirming that suppression of high turnover “stemness” factors contributes to its anti-cancer effects. SVC112 is a novel agent with promising efficacy in HNSCC.

Supplementary Material

Refer to Web version on PubMed Central for supplementary material.

Acknowledgements:

The authors wish to thank the patients who donated their tissue, blood and time, and to the clinical teams who facilitated patient informed consent, as well as sample and data acquisition.

Financial Support: This work was supported by NCI SBIR Contract HHSN261201500010C (to SuviCa.; subcontract to S.B.K.), P30-CA046934 (AJ, University of Colorado Cancer Center Support Grant), NIH R01 GM106317 (T.T.S.), R35 GM130374 (T.T.S.), Ruth L. Kirschstein National Research Service Award T32CA17468 (P.N.L. trainee), the Daniel and Janet Mordecai Foundation (A.J.), the Charles C. Gates Center for Stem Cell Biology (A.J.), and the Peter and Rhonda Grant Foundation (A.J.).

REFERENCES

1. Jemal A, Siegel R, Ward E, Hao Y, Xu J, Murray T, et al. Cancer statistics, 2008. CA Cancer J Clin 2008;58:71–96 [PubMed: 18287387]
2. Siegel RL, Miller KD, Jemal A. Cancer statistics, 2015. CA Cancer J Clin 2015;65:5–29 [PubMed: 25559415]
3. Kreso A, Dick JE. Evolution of the cancer stem cell model. Cell Stem Cell 2014;14:275–91 [PubMed: 24607403]
4. Keysar SB, Le PN, Miller B, Jackson BC, Eagles JR, Nieto C, et al. Regulation of Head and Neck Squamous Cancer Stem Cells by PI3K and SOX2. J Natl Cancer Inst 2017;109
5. Chen K, Huang YH, Chen JL. Understanding and targeting cancer stem cells: therapeutic implications and challenges. Acta Pharmacol Sin 2013;34:732–40 [PubMed: 23685952]
6. Vidal SJ, Rodriguez-Bravo V, Galsky M, Cordon-Cardo C, Domingo-Domenech J. Targeting cancer stem cells to suppress acquired chemotherapy resistance. Oncogene 2014;33:4451–63 [PubMed: 24096485]
7. Buszczak M, Signer RA, Morrison SJ. Cellular differences in protein synthesis regulate tissue homeostasis. Cell 2014;159:242–51 [PubMed: 25303523]
8. Bastide A, David A. The ribosome, (slow) beating heart of cancer (stem) cell. Oncogenesis 2018;7:34 [PubMed: 29674660]
9. Beck B, Blanpain C. Unravelling cancer stem cell potential. Nat Rev Cancer 2013;13:727–38 [PubMed: 24060864]
10. Yan C, Higgins PJ. Drugging the undruggable: transcription therapy for cancer. Biochim Biophys Acta 2013;1835:76–85 [PubMed: 23147197]
11. Gregory MA, Hann SR. c-Myc proteolysis by the ubiquitin-proteasome pathway: stabilization of c-Myc in Burkitt's lymphoma cells. Mol Cell Biol 2000;20:2423–35 [PubMed: 10713166]
12. Wiegering A, Uthe FW, Jamieson T, Ruoss Y, Huttenrauch M, Kuspert M, et al. Targeting Translation Initiation Bypasses Signaling Crosstalk Mechanisms That Maintain High MYC Levels in Colorectal Cancer. Cancer Discov 2015;5:768–81 [PubMed: 25934076]
13. Fang L, Zhang L, Wei W, Jin X, Wang P, Tong Y, et al. A methylation-phosphorylation switch determines Sox2 stability and function in ESC maintenance or differentiation. Mol Cell 2014;55:537–51 [PubMed: 25042802]
14. Cambridge SB, Gnad F, Nguyen C, Bermejo JL, Kruger M, Mann M. Systems-wide proteomic analysis in mammalian cells reveals conserved, functional protein turnover. J Proteome Res 2011;10:5275–84 [PubMed: 22050367]
15. Yi T, Kabha E, Papadopoulos E, Wagner G. 4EGI-1 targets breast cancer stem cells by selective inhibition of translation that persists in CSC maintenance, proliferation and metastasis. Oncotarget 2014;5:6028–37 [PubMed: 25115391]

16. Jaklevic B, Uyetake L, Lemstra W, Chang J, Leary W, Edwards A, et al. Contribution of growth and cell cycle checkpoints to radiation survival in Drosophila. Genetics 2006;174:1963–72 [PubMed: 17028317]
17. Gladstone M, Frederick B, Zheng D, Edwards A, Yoon P, Stickel S, et al. A translation inhibitor identified in a Drosophila screen enhances the effect of ionizing radiation and taxol in mammalian models of cancer. Dis Model Mech 2012;5:342–50 [PubMed: 22344740]
18. Stickel SA, Gomes NP, Frederick B, Raben D, Su TT. Bouvardin is a Radiation Modulator with a Novel Mechanism of Action. Radiat Res 2015;184:392–403 [PubMed: 26414509]
19. Lewis SM, Holcik M. IRES in distress: translational regulation of the inhibitor of apoptosis proteins XIAP and HIAP2 during cell stress. Cell Death Differ 2005;12:547–53 [PubMed: 15818406]
20. Spriggs KA, Stoneley M, Bushell M, Willis AE. Re-programming of translation following cell stress allows IRES-mediated translation to predominate. Biol Cell 2008;100:27–38 [PubMed: 18072942]
21. Holcik M, Sonenberg N. Translational control in stress and apoptosis. Nat Rev Mol Cell Biol 2005;6:318–27 [PubMed: 15803138]
22. Narayanan V, Gutman JA, Pollyea DA, Jimeno A. Omacetaxine mepesuccinate for the treatment of chronic myeloid leukemia. Drugs Today (Barc) 2013;49:447–56 [PubMed: 23914353]
23. Le PN, Keysar SB, Miller B, Eagles JR, Chimed TS, Reisinger J, et al. Wnt signaling dynamics in head and neck squamous cell cancer tumor-stroma interactions. Mol Carcinog 2019;58:398–410 [PubMed: 30378175]
24. Keysar SB, Astling DP, Anderson RT, Vogler BW, Bowles DW, Morton JJ, et al. A patient tumor transplant model of squamous cell cancer identifies PI3K inhibitors as candidate therapeutics in defined molecular bins. Mol Oncol 2013;7:776–90 [PubMed: 23607916]
25. Calviello L, Mukherjee N, Wyler E, Zauber H, Hirsekorn A, Selbach M, et al. Detecting actively translated open reading frames in ribosome profiling data. Nat Methods 2016;13:165–70 [PubMed: 26657557]
26. Alao JP. The regulation of cyclin D1 degradation: roles in cancer development and the potential for therapeutic invention. Mol Cancer 2007;6:24 [PubMed: 17407548]
27. Hall EJ, Giaccia AJ. Radiobiology for the Radiologist. 530 Walnut Street, Philadelphia, PA 19106 USA2006.
28. Truitt ML, Ruggero D. New frontiers in translational control of the cancer genome. Nat Rev Cancer 2017;17:332
29. Gandhi V, Plunkett W, Cortes JE. Omacetaxine: a protein translation inhibitor for treatment of chronic myelogenous leukemia. Clin Cancer Res 2014;20:1735–40 [PubMed: 24501394]
30. Chen Y, Hu Y, Michaels S, Segal D, Brown D, Li S. Inhibitory effects of omacetaxine on leukemic stem cells and BCR-ABL-induced chronic myeloid leukemia and acute lymphoblastic leukemia in mice. Leukemia 2009;23:1446–54 [PubMed: 19322212]
31. Huang MT. Harringtonine, an inhibitor of initiation of protein biosynthesis. Mol Pharmacol 1975;11:511–9 [PubMed: 1237080]
32. Fresno M, Jimenez A, Vazquez D. Inhibition of translation in eukaryotic systems by harringtonine. Eur J Biochem 1977;72:323–30 [PubMed: 319998]
33. Lee IH, Eisbruch A. Mucositis versus tumor control: the therapeutic index of adding chemotherapy to irradiation of head and neck cancer. Int J Radiat Oncol Biol Phys 2009;75:1060–3 [PubMed: 19304406]
34. Muller PY, Milton MN. The determination and interpretation of the therapeutic index in drug development. Nat Rev Drug Discov 2012;11:751–61 [PubMed: 22935759]
35. Caunt CJ, Keyse SM. Dual-specificity MAP kinase phosphatases (MKPs): shaping the outcome of MAP kinase signalling. FEBS J 2013;280:489–504 [PubMed: 22812510]
36. Wang J, Zhou JY, Kho D, Reiners JJ Jr., Wu GS. Role for DUSP1 (dual-specificity protein phosphatase 1) in the regulation of autophagy. Autophagy 2016;12:1791–803 [PubMed: 27459239]
37. Liu F, Gore AJ, Wilson JL, Korc M. DUSP1 is a novel target for enhancing pancreatic cancer cell sensitivity to gemcitabine. PLoS One 2014;9:e84982 [PubMed: 24409315]

38. Katsuoka F, Yamamoto M. Small Maf proteins (MafF, MafG, MafK): History, structure and function. Gene 2016;586:197–205 [PubMed: 27058431]

39. Zhao W, Sun M, Li S, Chen Z, Geng D. Transcription factor ATF3 mediates the radioresistance of breast cancer. J Cell Mol Med 2018;22:4664–75 [PubMed: 30117642]

40. Sethi G, Sung B, Aggarwal BB. TNF: a master switch for inflammation to cancer. Front Biosci 2008;13:5094–107 [PubMed: 18508572]

41. Hoesel B, Schmid JA. The complexity of NF-kappaB signaling in inflammation and cancer. Mol Cancer 2013;12:86 [PubMed: 23915189]

42. Zhou X, Liao WJ, Liao JM, Liao P, Lu H. Ribosomal proteins: functions beyond the ribosome. J Mol Cell Biol 2015;7:92–104 [PubMed: 25735597]

43. Fausto N Liver regeneration and repair: hepatocytes, progenitor cells, and stem cells. Hepatology 2004;39:1477–87 [PubMed: 15185286]

44. Maciejewski JP, Risitano A. Hematopoietic stem cells in aplastic anemia. Arch Med Res 2003;34:520–7 [PubMed: 14734092]

45. Tentler JJ, Tan AC, Weekes CD, Jimeno A, Leong S, Pitts TM, et al. Patient-derived tumour xenografts as models for oncology drug development. Nat Rev Clin Oncol 2012;9:338–50 [PubMed: 22508028]

Statement of Significance:

Inhibiting protein elongation with SVC112 reduces tumor growth in head and neck squamous cell carcinoma and increases the effects of radiation by targeting the cancer stem cell pool.

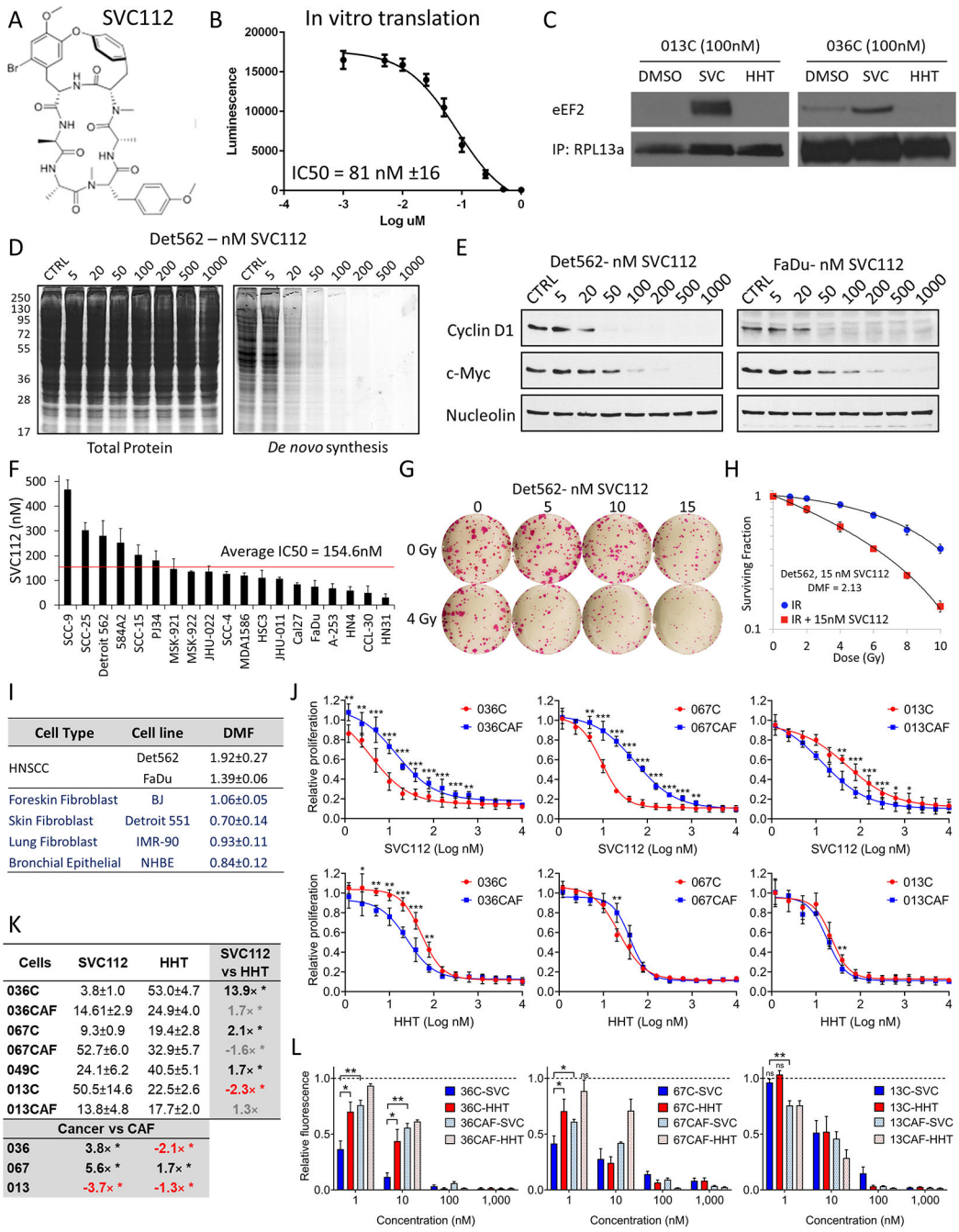

Cell Type	Cell line	DMF
HNSCC	Det562	1.92±0.27
	FaDu	1.39±0.06
Foreskin Fibroblast	BJ	1.06±0.05
Skin Fibroblast	Detroit 551	0.70±0.14
Lung Fibroblast	IMR-90	0.93±0.11
Bronchial Epithelial	NHBE	0.84±0.12

Cells	SVC112	HHT	SVC112 vs HHT
036C	3.8±1.0	53.0±4.7	13.9× *
036CAF	14.61±2.9	24.9±4.0	1.7× *
067C	9.3±0.9	19.4±2.8	2.1× *
067CAF	52.7±6.0	32.9±5.7	-1.6× *
049C	24.1±6.2	40.5±5.1	1.7× *
013C	50.5±14.6	22.5±2.6	-2.3× *
013CAF	13.8±4.8	17.7±2.0	1.3×
Cancer vs CAF			
036	3.8× *	-2.1× *	
067	5.6× *	1.7× *	
013	-3.7× *	-1.3× *	

Figure 1. SVC112 and its effect on protein translation and HNSCC cell lines.

(**A**) The chemical structure of SVC112, synthetic derivative of cyclic hexapeptide bouvardin. (**B**) SVC112 inhibits *in vitro* translation. Uncapped poly(A)+ luciferase mRNA was translated with rabbit reticulocyte lysates for 30 min at 30°C in the presence of increasing SVC112 concentrations. (**C**) Ribosomal protein RPL13a was magnetically separated (using RPL13a specific antibodies) from cell lysates following treatment with control (DMSO), 100nM SVC112 or 100nM HHT. Co-immunoprecipitation of eEF2 with RPL13a was assessed by western blot. eEF2 precipitated with RPL13a only in lysates of 013C and 036C

cells treated with SVC112. (**D**) SVC112 inhibits new protein synthesis in Det562 HNSCC cells. Cells were incubated for 1h in methionine free media, followed by the addition of L-azidohomoalanine (AHA, 50 μM final) plus the indicated SVC112 concentrations for 2h. Protein extracts were prepared, AHA containing proteins were labeled with Tetramethylrhodamine, extracts were resolved via SDS-PAGE, AHA containing proteins were visualized under UV excitation. Total protein was visualized with Coomassie staining. (**E**) SVC112 depletes Myc and Cyclin D1 in Det562 and FaDu HNSCC cells. Cells were incubated with the indicated SVC112 concentrations for 2h, protein extracts were prepared, subject to SDS-PAGE, and Western blotting was performed with the indicated antibodies. House-keeping protein nucleolin did not change and served as a loading control. (**F**) SVC112 IC50 in 19 HNSCC cell lines. Cells were treated with a range of SVC112 concentrations for 5 days, cell growth was then determined via CellTiter-Glo, and IC50 was calculated using non-linear regression. The IC50 ranged by 15-fold with an average of 155nM. (**G-H**) SVC112 mediated radio-modulation in clonogenic survival assays. (**G**) Det562 cells were seeded clonogenically, treated with a single dose of radiation and/or the indicated concentrations of SVC112 for 24h, cells were then placed in fresh media lacking drug and allowed to grow for 9 days. The IC50 for clonogenicity was lower with an IC50 for Det562 of ~15nM, versus ~280nM in proliferation assays. (**H**) Example clonogenic data and best fit curves for Detroit562, one drug dose, a range of radiation, and the calculated SVC112 mediated Dose Modifying Factor (DMF) of radiation for this individual experiment. (**I**) The average DMF values for two HNSCC and four 'normal' cell lines from experiments performed as in (G), with a range of SVC112 concentrations for each cell line. The DMFs for all non-transformed cells were significantly different relative to Detroit562 ($P<0.001$) and FaDu ($P<.005$) by Student's t-test. (**J**) Antiproliferative effects of SVC112 and HHT *in vitro* measured by the SRB assay. (**K**) IC50 values (nM) ± 95% CI for SVC112 and HHT calculated for cancer and CAF cell lines. For cancer vs CAF comparisons; bold/black values represent greater effect (fold difference, IC50) in cancer cells, while negative red/bold values represent greater inhibition in CAFs (fold difference, IC50). For SVC112 vs HHT comparisons black/bold represents a lower IC50 for SVC112. (**L**) SVC112 and HHT (1.5h treatment) significantly inhibit protein synthesis in HNSCC cells and immortalized cancer-associated fibroblasts (CAFs), derived from the same tumor as the corresponding cancer cell line, in a dose dependent manner as measured by the methionine analog incorporation assay (Click-iT). All concentrations of SVC112 and HHT (1-1,000nM) significantly decreased ($P\leq.05$) fluorescence in all cell lines compared to DMSO treated controls unless noted as not significant (ns). Greater than 75% inhibition was achieved at concentrations between 10 and 100nM for each compound, while SVC112 demonstrated more activity than HHT at 1nM in 036C and 067C cells. Graphed results are presented as the mean±SD of a minimum of three independent experiments. Statistical significance (J and L) was calculated by two-tailed Student's *t* test (* $P\leq.05$, ** $P\leq.01$, *** $P\leq.001$). HNSCC=head and neck squamous cell carcinoma, SVC=SVC112, HHT=homoharringtonine, CAF=cancer associated fibroblasts.

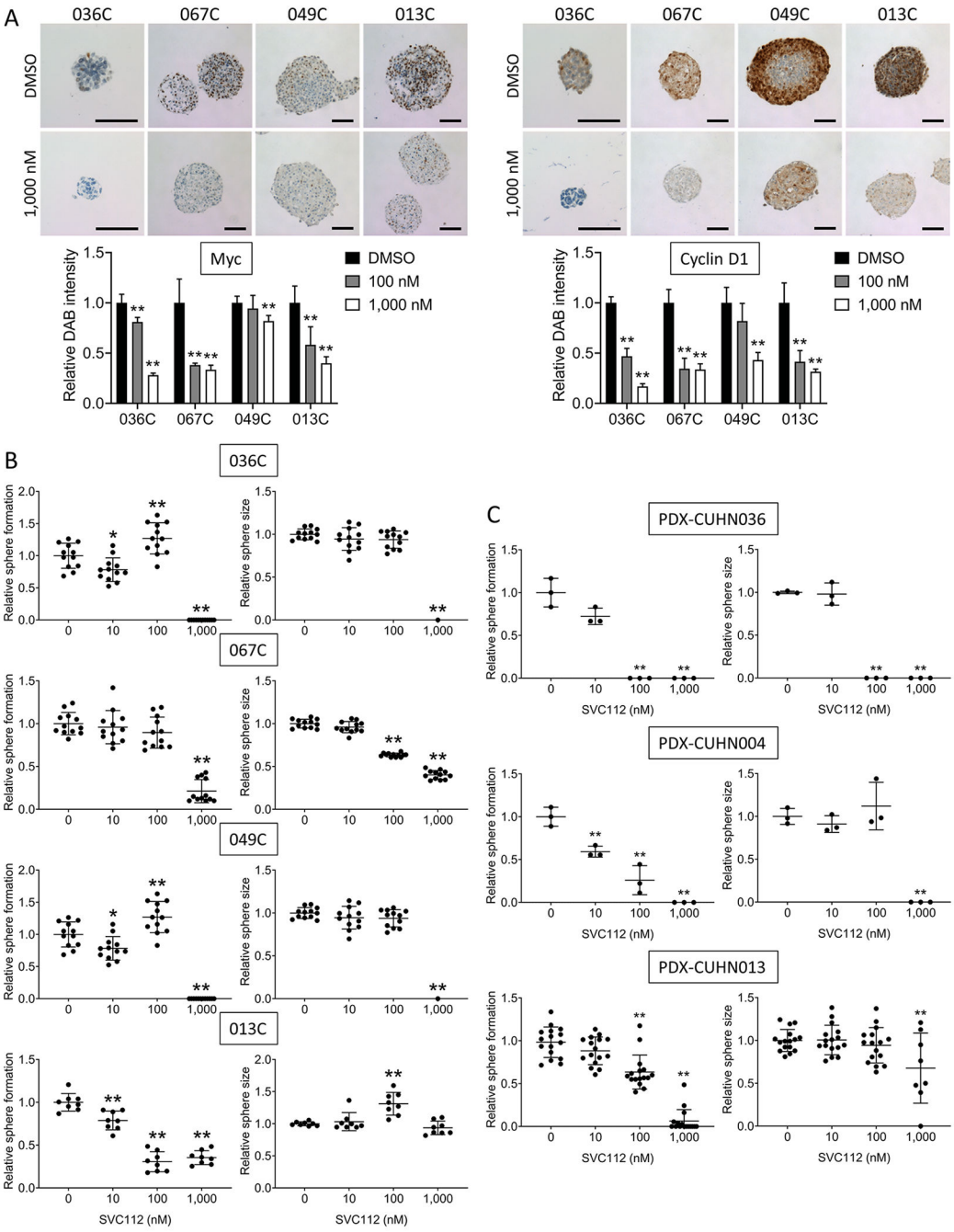

Figure 2. Effects of SVC112 CSC-related proteins and tumor sphere formation.

(**A**) Treating established cancer spheres (grown 10 days) with SVC112 (24h) suppresses levels of Myc and Cyclin D1 measured by IHC. Changes in DAB staining intensity was quantified using ImageJ Fiji. 036C 200x magnification, 067C, 049C, 013C 100x magnification, scale bars = 100μm. (**B**) SVC112 consistently decreases sphere formation by 013C (n=4, 16 wells), 036C (n=3, 12 wells), 049C (n=3, 12 wells), and 067C (n=3, 12 wells) HNSCC cell lines. Sphere size and number were quantified 10 days after seeding. (**C**) SVC112 decreases sphere formation by CSCs sorted from PDX tumors. Graphed results are

presented as mean ±SD. Statistical significance (B and C) was calculated by two-tailed Student's *t* test (* $P \leq .05$, ** $P \leq .01$). PDX=patient-derived xenograft, CSC=cancer stem cell, HNSCC=head and neck squamous cell carcinoma. IHC=immunohistochemistry.

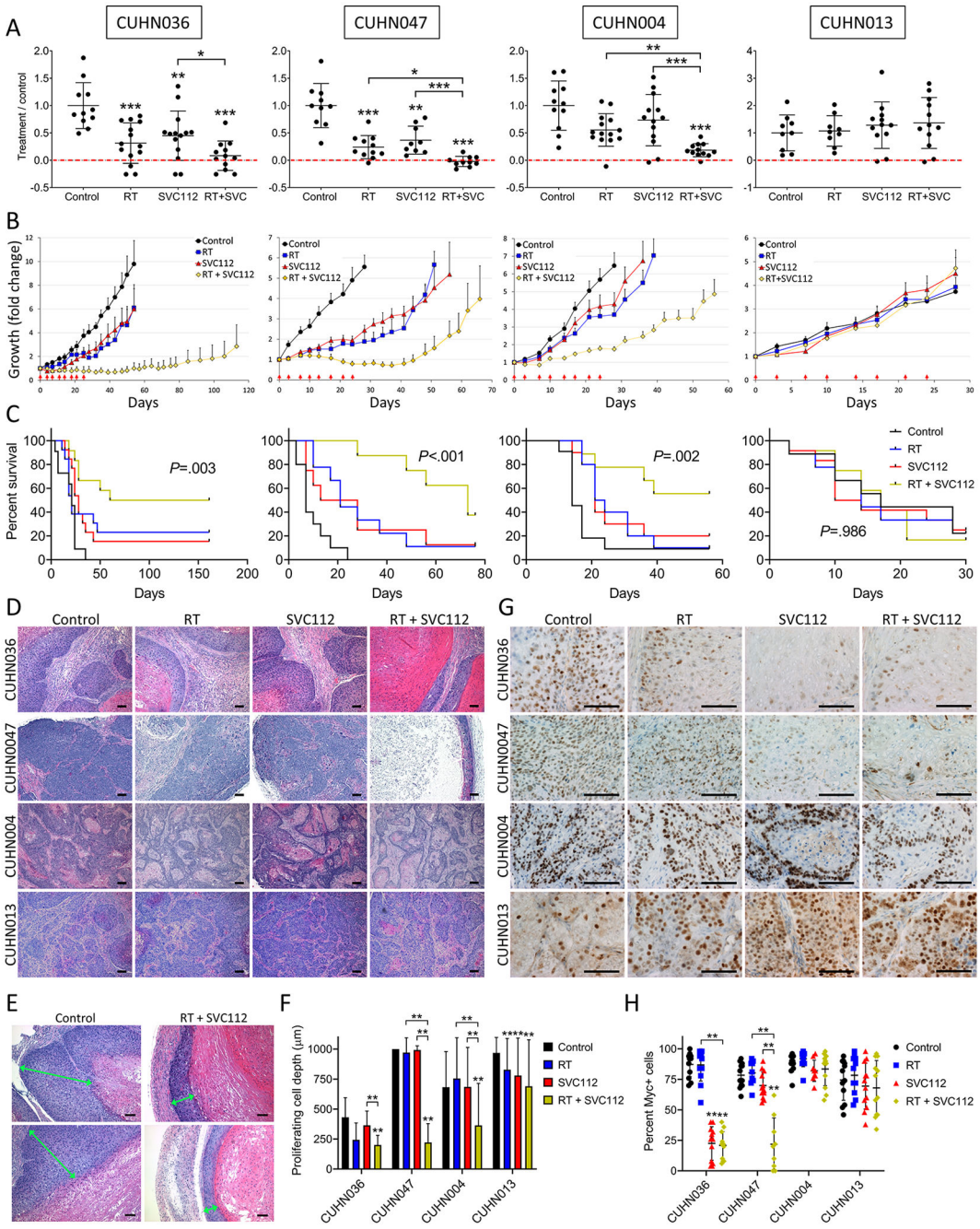

Figure 3. Efficacy of combination radiation and SVC112 treatment in HNSCC PDX models.

(**A and B**) CUHN036, CUHN047, CUHN004, and CUHN013 PDX models were treated with radiation and SVC112 alone and in combination. Tumor bearing animals were irradiated (3Gy) and treated with SVC112 twice weekly. SVC112 (60mg/kg) was delivered at the time of irradiation (0h) and 6h after irradiation. Red arrows indicate dosing days. (**A**) Treatment vs Control calculations for each tumor at day 28 of the study. Negative values (dashed red line) represent tumors that regressed with treatment (≥9 tumors per treatment arm). (**B**) CUHN036, CUHN047, CUHN004, and CUHN013 growth curves. CUHN036

regrowth: 2 of 8 tumors regressed completely, 4 of 8 tumors regressed to <75mm^3 and did not regrow, and 2 of 8 tumors were stable at the end treatment and eventually regrew. CUHN047 regrowth: 1 of 7 tumors regressed by the end of treatment and did not regrow, 4 of 7 tumors regressed by the end of treatment but eventually regrew, and 2 of 7 tumors were stable (fold change of 1.24 and 1.25) at the end of treatment and eventually regrew. (**C**) Kaplan-Meier curves for CUHN036 (P=.003), CUHN047 (P≤.001), CUHN004 (P=.002), and CUHN013 (P=.986) generated by scoring tumors that reached 500mm^3 as events. (**D**) HE staining; Combination treatment increased keratinization and necrosis in CUHN036, CUHN047, CUHN004, and CUHN013 treated tumors. 50x magnification, scale bars = 100μm. (**E**) Measurement of live cancer cell depth (CUHN036 tumors) from the proliferating tumor edge (green arrow) to large areas of keratinization and/or necrosis (HE staining). 50x magnification, scale bars = 100μm. (**F**) Quantification of live/proliferating cancer cell depth by measuring 10 representative regions of ≥3 tumors from each treatment arm. Distances of 1,000μm or more were scored as 1,000μm. (**G-H**) SVC112 alone or in combination with radiation significantly decreased Myc levels in CUHN036 and CUHN047, but not CUHN004 and CUHN013. Percentages were calculated by scoring 100 cells from 3 representative regions for ≥3 tumors from each treatment arm. 200x magnification, scale bars = 100μm. Graphed results are presented as mean ±SD or (B) ±SEM. Statistical significance (A, F, and H) was calculated by two-tailed Student's *t* test, or (C) by Log-rank Mantel-Cox test (* P≤.05, ** P≤.01 *** P≤.001). RT=radiation therapy, SVC=SVC112, HNSCC=head and neck squamous cell carcinoma, PDX=patient-derived xenograft, HE=hematoxylin eosin, IHC=immunohistochemistry.

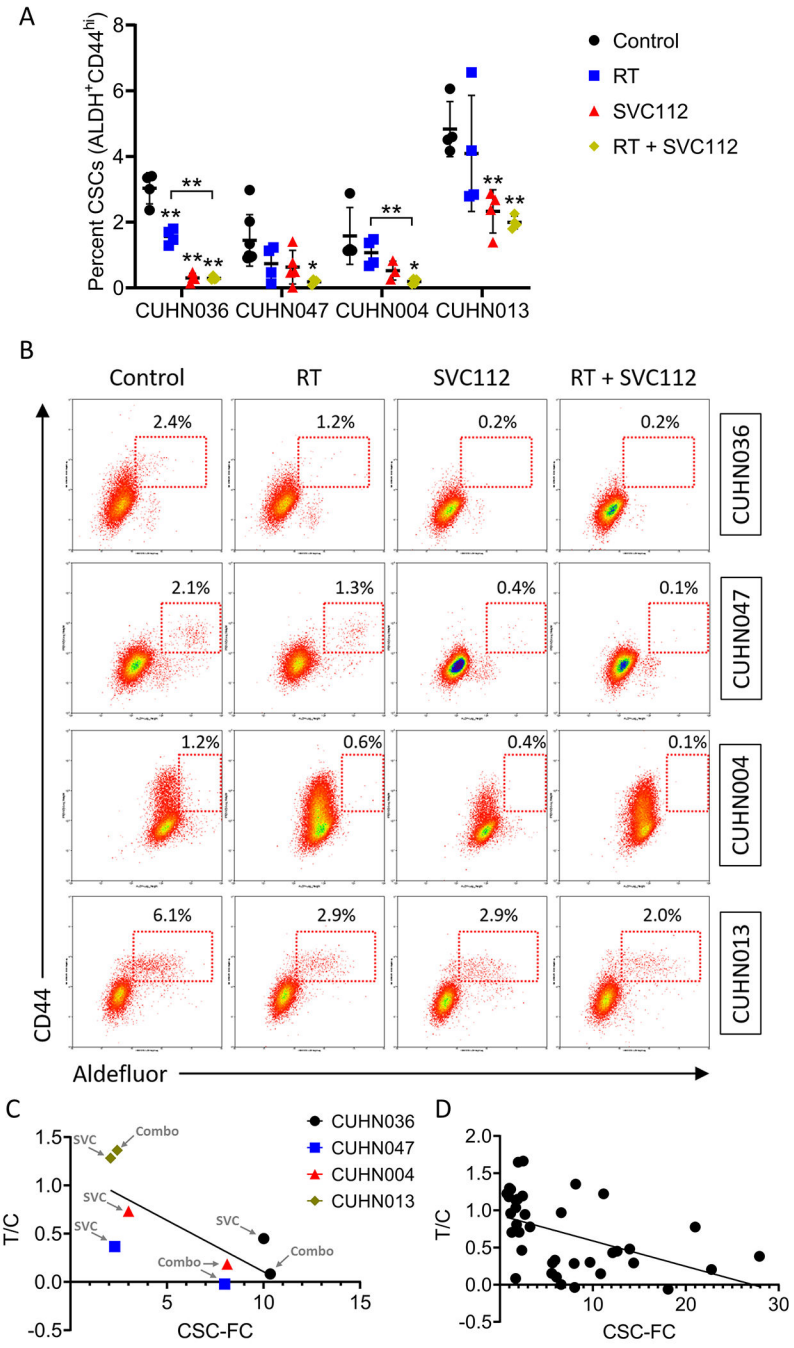

Figure 4. Relationship between SVC112 treatment and CSCs *in vivo*.

(**A**) SVC112 and combination treatment decreased the HNSCC CSC fraction (ALDH $^{+}$CD44^{high}) at day 28 in all PDX models. Graphed results are presented as mean ±SD. (**B**) Representative flow cytometry histograms of CSC populations (ALDH^{+}CD44^{high}) in control and treated tumors on day 28 of efficacy studies. (**C and D**) Relationship between tumor response (treatment/control) and decrease in the *in vivo* CSC population for SVC112 (SVC) and RT + SVC112 (Combo) treated tumors; **C** = average for tumors in the pooled SVC112 and combination (Combo) treatment arms (*P*=.037), **D** = values for each individual SVC112

or combination treated tumor (P=.002). Statistical significance (A) was calculated by two-tailed Student's t test or (C and D) by linear regression (* $P \leq .05$, ** $P \leq .01$). CSC=cancer stem cell, HNSCC=head and neck squamous cell carcinoma. ALDH=aldehyde dehydrogenase, RT=radiation therapy, T/C=treatment/control, FC=fold change.

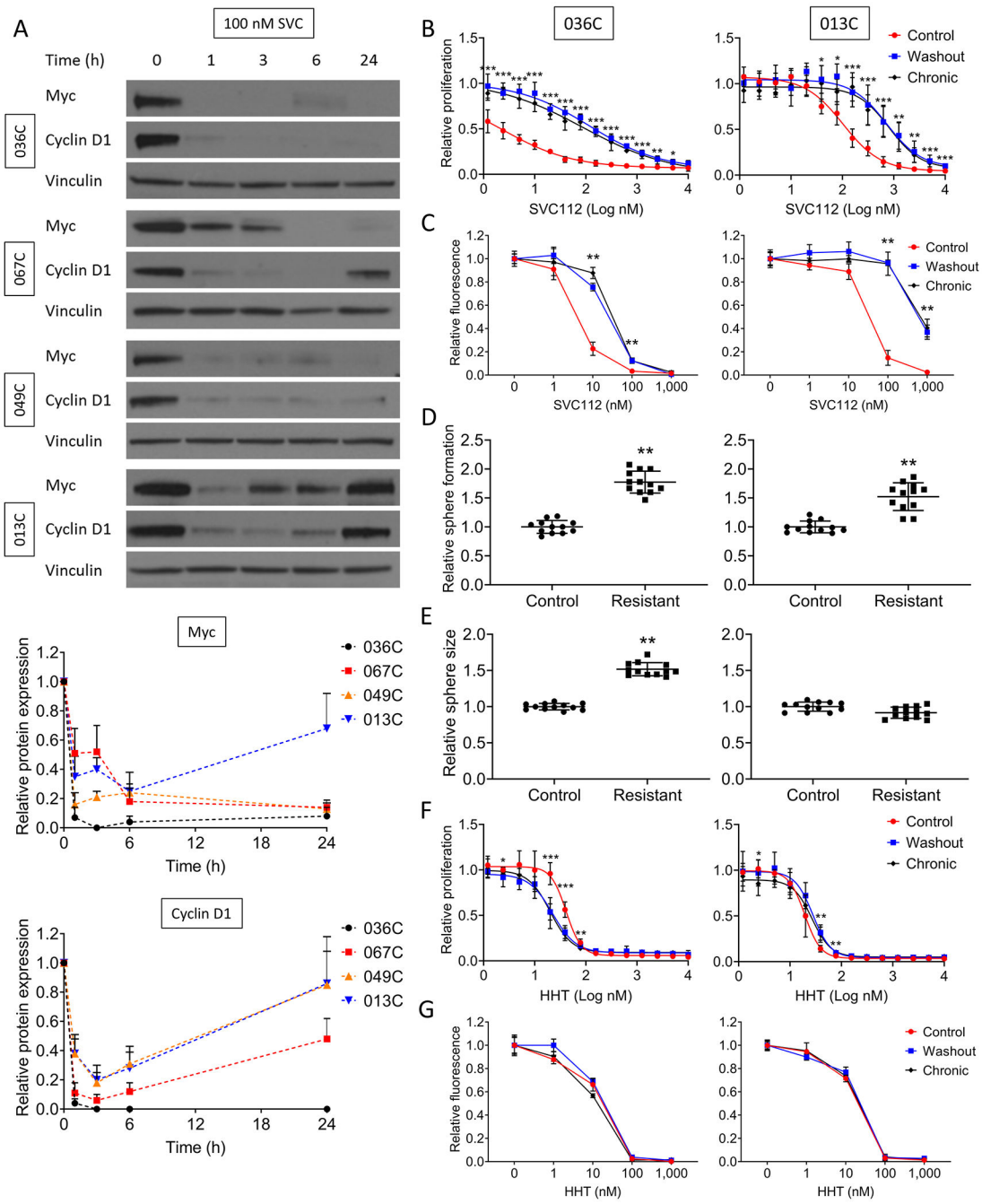

Figure 5. Analysis of SVC112 resistance.

(**A**) SVC112 consistently decreases Myc and Cyclin D1 levels within 1h of treatment. (Top) representative western blots and (Bottom) densitometry analysis for Myc and Cyclin D1 over time ($n \geq 3$ blots from independent experiments). (**B**) SRB assay of control and SVC112 resistant cells treated with SVC112. (**C**) Inhibition of protein synthesis by SVC112 in control (DMSO) and SVC112 resistant cell lines that were continuously cultured in SVC112 prior to the assay (chronic) or washed out of drug seven days prior (washout). (**D**) Sphere formation and (**E**) sphere size for control and SVC112 resistant cell lines. (**F**) SRB assay of

control and SVC112 resistant cells treated with HHT. (**G**) Click-iT analysis of HHT treatment on control and SVC112 resistant (washout and chronically treated) 036C and 013C cell lines. Graphed results are presented as mean ±SD. Statistical significance was calculated by two-tailed Student's *t* test (* $P \leq .05$, ** $P \leq .01$). SRB=sulforhodamine B colorimentric assay, HHT=homoharringtonine. SVC=SVC112.

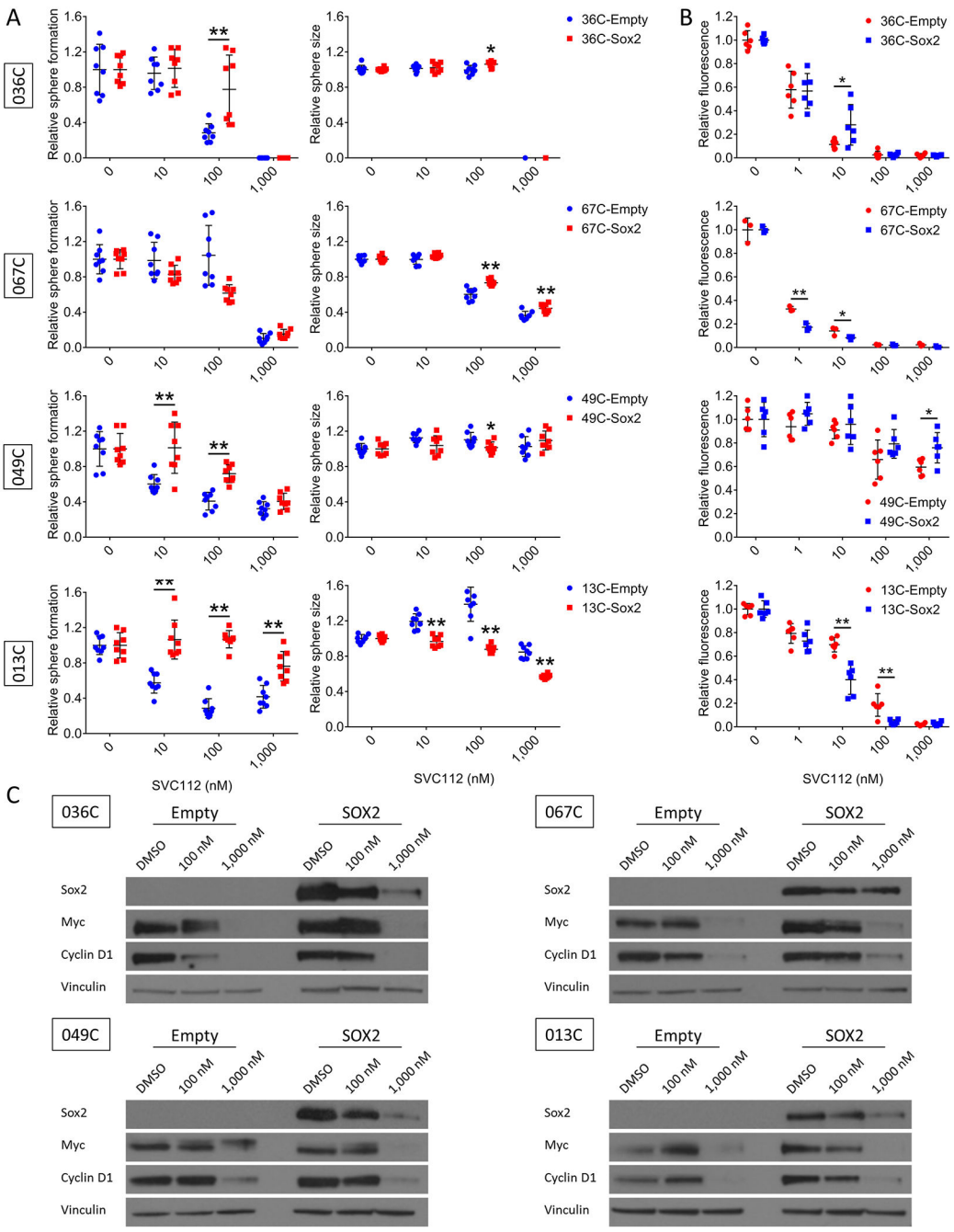

Figure 6. Effects of exogenous Sox2 expression of SVC112 treatment.

(**A**) 013C, 036C, and 049C cells expressing Sox2 are less sensitive to the anti-sphering effects of SVC112 treatment. (**B**) Sox2 expression does not dramatically alter the ability of SVC112 to suppress protein synthesis in HNSCC cell lines, as measured by methionine analog incorporation (Click-iT). (**C**) Western blot analysis of control vector (Empty) and Sox2 expressing cell lines treated with SVC112 (24h). Graphed results are presented as mean ±SD. Statistical significance was calculated by two-tailed Student's *t* test. (* $P \leq .05$, ** $P \leq .01$).

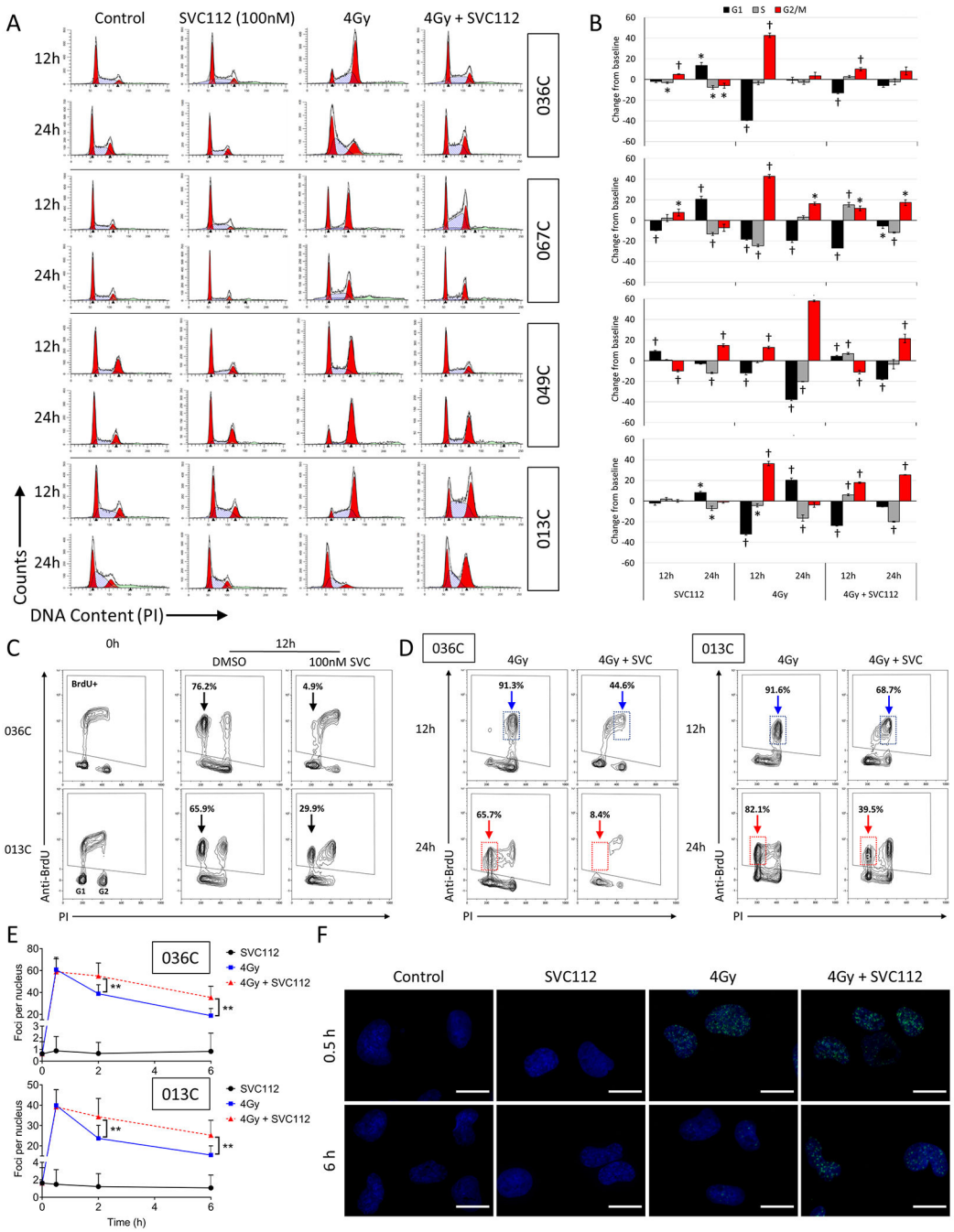

Figure 7. Effect of SVC112 on cell cycle checkpoints and DNA repair following radiation in HNSCC cells.

(**A-B**) Cell cycle analysis of 013C and 036C cell lines treated with radiation (4Gy), SVC112 (100nM) or combination radiation + SVC112. (**A**) Representative cell cycle histograms for 036C, 067C, 049C, and 013C at 12h and 24h following treatment. SVC112 delayed the G2/M arrest in when added to cells immediately following irradiation. (**B**) Change in the fraction of cells in each phase of the cell cycle following treatment, compared to the untreated (baseline of 0) control. (**C**) Prior to treatment, cells were pulse labeled with BrdU

for 1h, which consistently resulted in BrdU-positive populations between 48-52% for both 013C and 036C. 12h post labeling 65.9% of 013C and 76.2% of 036C BrdU-positive control cells had divided (G1 DNA content), while only 29.9% and 4.9% of SVC112 treated 013C and 036C cells were able to divide (black arrows). (**C**) 013C and 036C cells were treated with 4Gy radiation or 4Gy plus SVC112 (100nM). Addition of SVC112 delayed the accumulation and retention of cells at the G2/M checkpoint (blue arrows/gates) compared to radiation alone at 12h and 24h following treatment. 24h after radiation alone, 82.1% (013C) and 65.7% (036C) of BrdU-positive cells had cleared the G2/M arrest. However, combination treatment decreased the number of BrdU-positive cells with G1 DNA content to 39.5% and 8.4% for 013C and 036C cells respectively. (**D**) Effects of SVC112 on radiation induced γH2AX foci formation and resolution. Quantification of γH2AX foci per nuclei at 0.5h, 2h, and 6h following radiation (4Gy) +/− SVC112 (100nM) in 013C (n=3, 50 nuclei per experimental replicate) and 036C (n=3, 50 nuclei per experimental replicate) cell lines. Radiation plus SVC112 delayed loss of foci in both cell lines when compared to radiation alone. (**E**) Representative images of γH2AX foci in the nuclei of 036C cells. 1,008x magnification, scale bars = 20μm. Graphed results are presented as mean ±SD for three independent experiments. Statistical significance was calculated by two-tailed Student's t test (* P≤.05, ** P≤.01). SVC=SVC112, BrdU=bromodeoxyuridine, γH2AX=phosphorylated H2A.X variant histone.